Journal of Power Sources 196 (2011) 8280–8285

Contents lists available at ScienceDirect

Journal of Power Sources

journal homepage: www.elsevier.com/locate/jpowsour

Proton transport, water uptake and hydrogen permeability of nanoporous hematite ceramic membranes

M.T. Colomer*

Instituto de Cerámica y Vidrio, CSIC, C/Kelsen n° 5, Campus de la Universidad Autónoma, 28049 Madrid, Spain

ARTICLE INFO

Article history:
Received 16 February 2011
Received in revised form 27 May 2011
Accepted 3 June 2011
Available online 13 June 2011

Keywords:
Hematite ceramic membranes
Mesoporosity
Electrolyte
Proton exchange membranes
PEMFCs

ABSTRACT

For the first time, mesoporous acid-free hematite ceramic membranes have been studied as proton conductors. The xerogels after calcination at 300 °C for 1 h were mesoporous, as is mentioned above, with a BET surface area of $130 \pm 2\ m^2\ g^{-1}$, an average pore diameter of 3.8 nm and a pore volume of $0.149 \pm 0.001\ cc\ g^{-1}$. A sigmoidal dependence of the conductivity and the water uptake with the RH at a constant temperature was observed. The conductivity of the ceramic membranes increased linearly with temperature for all relative humidities studied. The highest value of proton conductivity was found to be $2.76 \times 10^{-3}\ S\ cm^{-1}$ at 90 °C and 81% RH. According to the activation energy values, proton migration in this kind of materials could be dominated by the Grotthuss mechanism in the whole range of RH. The low cost and high hydrophilicity of these ceramic membranes make them potential substitutes for perfluorosulfonic polymeric membranes in proton exchange membrane (PEMFCs). In addition, since hydrogen permeability values are in the range of 10^{-9} to $10^{-10}\ mol\ cm^{-1}\ s\ Pa$, in order to fabricate oxide-based PEMs that are capable of keeping streams of H_2 and O_2 from mixing, a separation layer with pore sizes <2 nm whose pores are filled with water will be needed.

1. Introduction

It is well known that α-Fe_2O_3 (hematite) nanoparticles are particularly appealing for experimental and theoretical investigations in view of their technological applications. In fact, they have been widely used as red pigments, catalysts in dehydrogenation reactions, anticorrosive agents, and starting materials in the synthesis of magnetic ferrites [1–4]. Their applications in nonlinear optics, gas sensors and in solar energy conversion and storage have also been recently investigated [5,6]. Nevertheless, if α-Fe_2O_3 is prepared as a mesoporous membrane it could behave as a proton conducting material and to the best of my knowledge, hematite has not been studied yet as a proton conductor. At present, Nafion is one of the few materials that deliver the set of chemical, electrochemical and mechanical properties required to perform as a good electrolyte in PEMFCs [7]. However, Nafion® membranes are very expensive, hard to synthesize and present environmental problems with regard to recycling and disposal of fluorinated polymers and their separation from the platinum catalysts used. In addition, polymer and hybrid membranes are susceptible to deformation on the basis of their repetition of sorption, desorption, and permeation of water. The deformation increases the interfacial resistance between the membrane and electrodes, and decreases the fuel cell performance. Moreover, the detrimental problem for high temperature use of Nafion is the loss of grafted HSO_4 branches as well as the loss of its good mechanical properties [8]. Over the last ten years, the proton conductivity characteristics of porous P_2O_5–SiO_2 glasses, xerogels, ceramic membranes, solid acids, and ordered mesoporous silica membranes have been the subject of growing interest due to their potential as solid electrolytes in sensors, fuel cells, etc. [9–22]. However, the application of solid acids as electrolytes in a fuel cell requires lower thicknesses than they show, i.e., 1.5 mm [20]. In addition, a subsequent study has indicated that this type of materials may be not stable in fuel cell environments [21]. The same problem of instability affects to the glasses based on phosphates [10]. Ordered mesoporous MCM-41 silica with assembled $H_3PW_{12}O_{40}$ nanoparticles by the vacuum-assisted impregnation method have been prepared and showed proton conductivity values of 1.8×10^{-2} and $4.5 \times 10^{-2}\ S\ cm^{-1}$ at 25 and 150 °C, respectively. However, a drastic and rapid decrease in conductivity occurs as a function of time due to a partial or a total loss of the impregnated acid [22].

Possible future electrolyte materials in PEMFCs should provide high and constant proton conductivity at low temperature; hydrophilicity and mechanical, thermal, and chemical stability under fuel cell conditions. They should also be impermeable to H_2 and O_2. Stable inorganic xerogels and/or ceramic membranes with high conductivities at low temperature, if developed, would

* Tel.: +34 91 735 58 40; fax: +34 91 735 58 43.
E-mail address: tcolomer@icv.csic.es

0378-7753/$ – see front matter © 2011 Elsevier B.V. All rights reserved.
doi:10.1016/j.jpowsour.2011.06.018

extend usefulness beyond the limitation of organic and hybrid films, glasses, solid acids, and acid-impregnated membranes, and would have potential viability. A totally inorganic membrane electrolyte approach to solving the high temperature problem could be the use of mesoporous acid-free oxide exchange ceramic membranes with an average pore size higher than 2 nm and lower than 10 nm [14,17,19].

The use of these mesoporous membranes would require tube or flat technology fuel cell geometry to avoid contact between cathode and anode reagents. Furthermore, in order to fabricate oxide-based PEMFCs that are capable of keeping streams of H_2 and O_2 from mixing, a separation layer with an average pore size with an average pore size <2 nm whose pores are filled with water would be necessary. α-Fe_2O_3 nanoparticles loaded with Pt will be employed as the electrodes. The membrane electrode assemblies could be prepared by dip-coating, spin-coating or slip-casting techniques.

The sol–gel method is an excellent process for producing highly proton-conductive solid materials, since the control of pore structure such as pore diameter and pore volume keeping the isotropy of the porous network is very important for designing the proton conducting paths.

The objective of this work is to design mesoporous acid-free hematite ceramic membranes of high pore volume and small pore size (3.8 nm) by a sol–gel route assisted by microwaves, with the aim of obtaining proton exchange electrolytes for PEMFCs. A study of the electrical transport properties and water uptake behavior as a function of both temperature and relative humidity is also reported.

2. Experimental

2.1. Synthesis of the α-Fe_2O_3 ceramic membranes

The ferric oxide sol was prepared by weak-base titration ($NaHCO_3$, Mallinckrodt, USA) of a fresh ferric nitrate solution ($Fe(NO_3)_3{\cdot}9H_2O$, Fisher Scientific, USA). The nitrate was dissolved in Milli-Q water and filtered through a 0.2 μm nucleopore filter (Millipore, USA). A titration rate of 2.5 ml min^{-1} under conditions of rapid stirring and room temperature resulted in the formation of a deep red, optically transparent solution at 15 min after starting the reaction. The hydrolytic solution was then microwaved at 100 °C using a Perkin–Elmer Multiwave 2000 system microwave oven (Waltham, MA, USA), and then quenched in ice-water. This treatment is expected to increase polymer stability toward growth and degradation by accelerating condensation reactions within the polymer structure and producing a "hardened and more flexible" polymer. The hydrosols were dialyzed in a membrane tubing: Spectra/por, molecular cut-off = 3500 molecular weight) against Milli-Q water until the pH was 4.0. The sol was then concentrated by rotary vaporization until a 0.62 M [Fe^{III}] sol was obtained. Bulk xerogel samples were obtained by drying the solution in Teflon dishes at 25 °C and at constant RH. Those xerogels were fired in air at 300 °C for 1 h.

2.2. Structural, textural and microstructural characterization

The fired bulk samples were employed to characterize the crystalline phase, texture and microstructure using X-ray diffractometry (XRD), Fourier transform infrared spectroscopy (FTIR), nitrogen sorption, and transmission electron microscopy-energy dispersive X-ray (TEM-EDX) techniques.

XRD analysis of powdered xerogels was carried out with a D-5000 Siemens (Karlsruhe, Germany) diffractometer using Ni-filtered Cu Kα radiation over a range of $15^\circ \leq 2\theta \leq 60^\circ$ at a step scan rate of $0.05^\circ\ s^{-1}$ collected at room temperature.

Fourier transform infrared (FTIR) spectroscopy was conducted between 4000 and 400 cm^{-1} on powdered xerogels mixed with KBr. The IR spectra were obtained with a Perkin–Elmer 1760X spectrophotometer (Waltham, Massachusetts, USA) with a 3600 data station, using the standard program CDS-13 for data handling. The porous structure of the membranes was characterized by nitrogen sorption (Micromeritics ASAP 2000 poresizer, Norcross, Georgia, USA) after degassing at 200 °C. N_2 with molecule cross-sectional area of 0.162 nm^2 was used as the adsorptive gas. Prior to N_2 sorption, all samples were degassed (i.e. exposing the monoliths to a vacuum pressure lower than 1 Pa at 200 °C overnight). The specific surface areas were estimated in relation to the masses of the outgassed samples. Three isotherms were collected for each sample to ensure that the data were representative. Pore size distributions were calculated from the desorption data using the BJH method [23,24]. Specific surface area was calculated from the BET equation. Pore volume was determined from the adsorption maxima. The mean coordination number Z (connectivity), and the linear dimension of the network, L, of the membranes was calculated from the hysteresis of the isotherms employing the Seaton's model based on the use of the percolation method [25].

The microstructure was studied by means of Transmission Electron Microscopy (TEM) and selected area electron diffraction (SAED) performed on a Jeol 2000FX microscope (Tokyo, Japan) working at 200 keV. Local composition was analyzed by EDAX with an ISIS analyzer system attached to the above mentioned microscope.

2.3. Water uptake studies

The total water content (chemisorbed + physisorbed) of the ceramic membranes was measured by thermogravimetric analysis (TG/DTG) using a Perkin–Elmer, Model Pyris 1 (Waltham, Massachusetts, USA). Samples were equilibrated at 81% RH before placing them in the balance crucible in order to reach full surface hydroxylation/hydration. Next, TG curves were registered under a dynamic dry air atmosphere of 20 ml min^{-1} up to 299 °C at a heating rate of 1 °C min^{-1}.

Physisorbed water in the xerogels was measured at 25 °C and 40 °C as a function of RH. The samples were kept in a closed thermostatic chamber with the desired RH maintained by saturated solutions of the appropriate salts [$MgCl_2{\cdot}6H_2O$ for 33%, $NaBr{\cdot}2H_2O$ for 58%, NaCl for 75%, $(NH_4)_2SO_4$ for 81% and K_2SO_4 for 97% RH] [26]. Samples were left to equilibrate at each RH for 24 h. The weight of the equilibrated samples was measured using a Mettler Toledo AT 261 Delta Range (Canton, MA, USA) balance place inside the chamber.

2.4. Electrical characterization and H_2 permeability

A hydrogen concentration cell was constructed to determine if proton are mobile species in these ceramic membranes. Both surfaces of the ceramic membranes were covered with porous Ag paste (area: 0.28 cm^2) and sealed by epoxy resin. The electromotive force generated between the electrodes was measured by a potentiostat (EG&G M-273A Instrument, Princeton Applied Research, USA) as a function of the hydrogen partial pressure. The total pressure of gases was constant at 1 atm and the gas flow rates were 150 ml min^{-1}. Both gases were moist and kept at a RH of 81% and at room temperature.

Electrical conductivity of the membranes was measured by electrochemical impedance spectroscopy (EIS) using a HP-4192A frequency response analyzer (Palo Alto, CA, USA). The frequency range used was 5–10^7 Hz. Gold electrodes (area: 0.28 cm^2) were sputtered onto both sides of each membrane prior to the electrical measurements. Before collecting impedance spectra, the

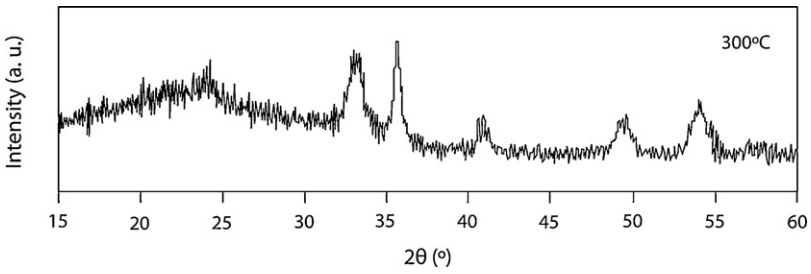

Fig. 1. XRD pattern of the α-Fe_2O_3 ceramic membrane after calcination at 300 °C for 1 h.

calcined membranes were allowed to equilibrate at different RH (33, 58, 75, 81 and 97%) for 24 h in sealed chambers containing the saturated solutions of appropriate salts mentioned above. Measurements were performed at constant temperature (from 25 to 90 °C), with the sample chamber immersed in a thermostatically controlled water bath. The reproducibility of the results was verified by repeating the measurements three times for a given sample, and also by testing different samples equilibrated under the same conditions. The spectra were fit using the EQUIVCRT program by Boukamp [27].

The hydrogen permeability was measured using a forced-convection drying oven (DO-600FA), under dry conditions, consisting of two compartments with a capacity of 50 cm^3. The chambers were separated by a vertical membrane with an effective area of 20 cm^2. All experiments were carried out in a temperature range of 25–100 °C at a pressure of 1 atm.

The samples for the H_2 permeability, electrical measurements and for the study of the water uptake were flat with a thickness of 0.10 cm.

3. Results and discussion

3.1. Structural, textural and microstructural characterization

The XRD pattern of the xerogel calcined at 300 °C for 1 h corresponds to hematite, α-Fe_2O_3 (PDF 33-0664). The peak broadening is very wide indicating a small crystallite size (Fig. 1).

The 525 cm^{-1} and 466 cm^{-1} peaks of the FTIR spectrum (not shown here) for the calcined xerogel lie within the transverse and longitudinal mode frequency range for two characteristic vibrations in hematite [28]. When the xerogels after calcination are crushed with an agate mortar and observed by TEM, agglomerates of individual crystals could be clearly perceived (Fig. 2). The resulting powder shows a particle size of ~5 nm. The selected area electron diffraction diagram (SAED) shown as an inset in the micrograph provides also a direct evidence of the microstructure of the materials, showing in this case a typical diffraction pattern of a polycrystalline sample (diffraction rings instead of well defined spots), in accordance with the XRD patterns.

The N_2 adsorption–desorption isotherm for the xerogels calcined at 300 °C for 1 h is of type IV of the IUPAC classification, and exhibits an *E* hysteresis loop in accordance with de Boer [29] or type H2 from IUPAC classification [30] (Fig. 3). The parameters of the connectivity for the membranes prepared in this work are $Z = 2.3 \pm 0.1$ and $L = 4.7 \pm 0.1$ according to the Seaton's model [25] indicating an open framework with an interconnected internal structure. Interconnection between pores is indispensable for achieving high proton conductivity.

The membranes were mesoporous, with a BET surface area of $130 \pm 4\ m^2\ g^{-1}$, an average pore diameter of 3.8 nm (desorption branch) (Fig. 4) and a pore volume of $0.149 \pm 0.001\ cm^3\ g^{-1}$.

3.2. Water uptake studies

As the RH is controlled by using saturated salts, and the % RH for these salts depends on temperature, the conductivity for the system from 40 to 90 °C may correspond to a lower RH.

Calcined α-Fe_2O_3 xerogels at 300 °C exposed to water vapor will have molecular water or hydroxyl groups coordinated to surface five-coordinated Fe^{3+} ions and hydroxyl groups coordinated to bridging O_2^- ions (chemisorbed water). These mesoporous materials should also have water molecules hydrogen bonded (physisorbed water) to bridging O_2^- ions of the surface (second layer water) and to other hydrogen bonded water molecules (multilayer water). Physisorbed and chemisorbed water should evolve at different temperatures [31,32] and each type of water can be calculated by the combination of TG and water adsorption studies.

From TG results the number of total water molecules per unit of specific surface area was calculated. These calculations show that,

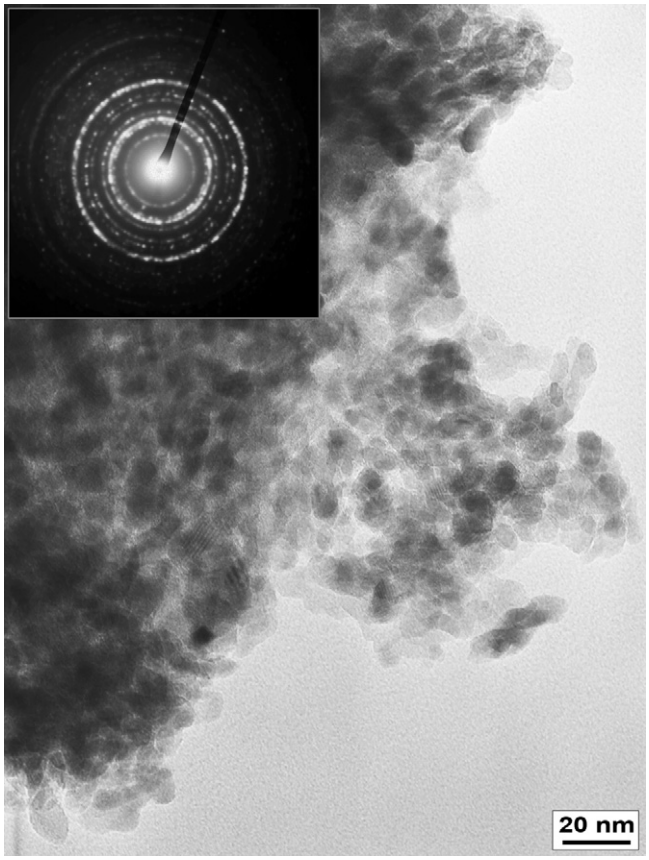

Fig. 2. TEM micrograph of the crushed xerogel after calcination at 300 °C for 1 h. Selected area electron diffraction pattern is shown in the inset.

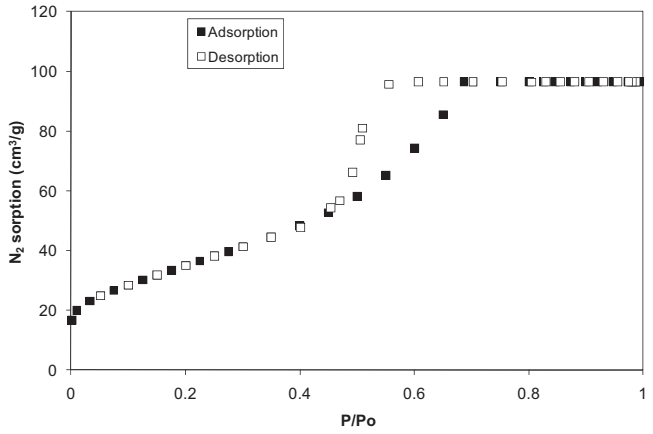

Fig. 3. Nitrogen adsorption–desorption isotherm of the hematite xerogel after calcination at 300 °C for 1 h.

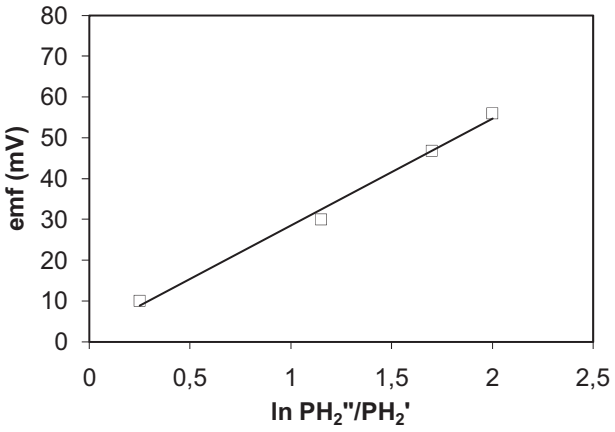

Fig. 6. Relationship between emf and relative hydrogen gas pressure at room temperature and 81% RH.

at 81% RH (atmosphere that the xerogel experiences for 24 h before the TG measurement) and from 25 to 299 °C the total number of water molecules (chemisorbed + physisorbed) per square nanometer is 32 molecules nm^{-2}.

The water adsorption isotherm of the xerogels normalized with respect to the specific surface area, i.e., the total water density as a function of the RH at 25 and 40 °C versus different RH in the hydrated xerogels is shown in Fig. 5. Since the outgassing of the samples prior to measuring the isotherms was done at 60 °C, the chemisorbed water was not removed and therefore the isotherms include only the physisorbed water. The shape of the isotherm is indicative of porous materials with surface polar groups [30], as is expected for metal oxides with coordinated water and hydroxyl surface groups. The adsorption at RH below 60% can be associated to the formation of a layer of water clusters and, at higher RH to the filling of the pores [33]. In other words, the sigmoidal trend of the isotherm could testify that the uptake of physisorbed water is a two-regime process. This mechanism was proposed by Dubinin and Serpinsky (D.S. theory) [33]. At lower RH, the water forms a layer of clusters along the walls of a matrix of interconnected pores. At higher RH, new water molecules start filling the remaining pore space through capillary condensation, and a saturation effect is observed at ~81% RH, i.e., this sample is almost fully water saturated in atmospheres with RH superior to 81%. Actually, the amount of water increases significantly as the RH is increased up to 81%. After this value, the amount of water increases very slightly for higher RH. This means than for higher RH the number of molecules per nm^2 is almost the same and equal to 24.4 molecules nm^{-2} indicating a saturation effect as a consequence of the sigmoidal trend of the water uptake. The difference between the total number of water molecules per nm^2 obtained from the TG analysis and the number of physisorbed ones obtained from the water adsorption isotherms will give us the number of chemisorbed water per square nanometer up to 299 °C, i.e., 32–24.4 = 7.6 molecules nm^{-2} at 25 °C.

The physisorbed water content values for the isotherm at 40 °C show that the water content is the same at both temperatures.

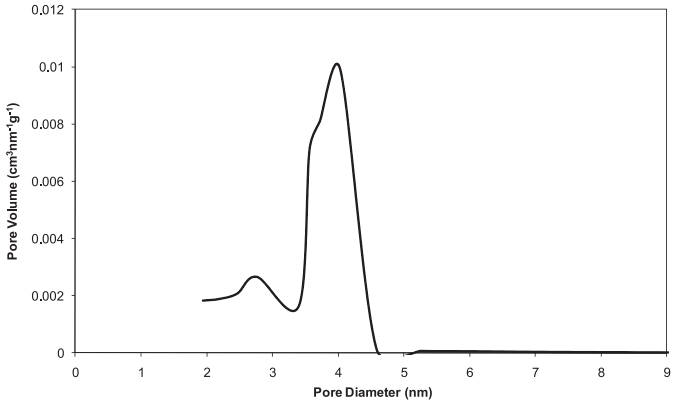

Fig. 4. Pore size distribution of the hematite xerogel after calcination at 300 °C for 1 h.

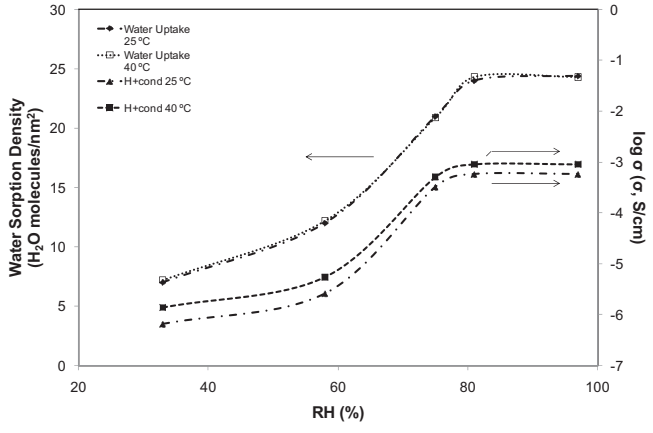

Fig. 5. Water adsorption isotherms (molecules of $H_2O\,nm^{-2}$) and proton conductivity, at 25 and 40 °C, versus relative humidity.

3.3. Electrical characterization and H_2 permeability

Fig. 6 shows the emf values at steady state as a function of the logarithm of hydrogen partial pressure that were obtained for the membrane. From that figure and also from the Nernstian equation it is possible to estimate the proton transport number of the hematite membrane. The emf values satisfied a linear relationship between emf and $\log p''H_2/p'H_2$. The constant number in the Nernstian equation is estimated 1.74 ± 0.03. This value is close to a theoretical value of 2, indicating that hydrogen reacts according to the reaction $H_2 = 2H^+ + 2e^-$, and the protons travel through the xerogel. This interpretation is in agreement with Nogami et al. [34] and Colomer and Anderson [14] who obtained an estimated value of 2.2 and 1.7 for porous sol–gel derived glasses of $P_2O_5{\cdot}SiO_2$ and silica xerogels, respectively.

Fig. 5 also shows the proton conductivity values at 25 °C and 40 °C measured at different RH values. The dependence of the conductivity in both cases has a sigmoidal trend like the physisorbed isotherms, however, as is expected, the values of proton conductiv-

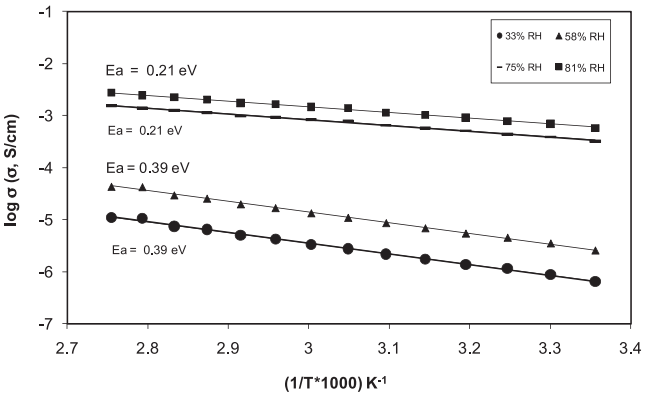

Fig. 7. Proton conductivity versus the reciprocal of the temperature at different RH for the α-Fe_2O_3 ceramic membranes.

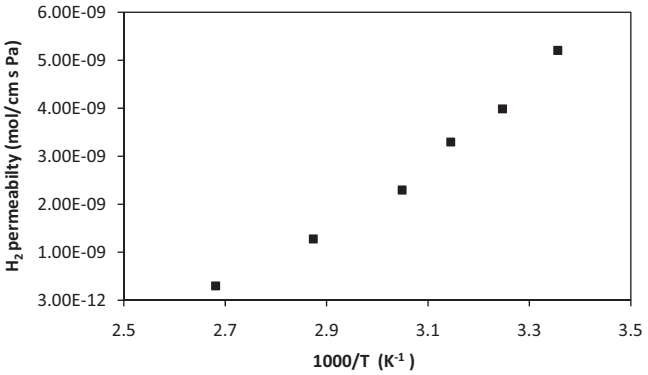

Fig. 8. Hydrogen permeation rate as a function of the reciprocal of the temperature.

ity are higher when the temperature increases, unlike the values of the water physisorbed. It is due to the fact that at higher temperatures the mobility of the charge carriers is higher.

According to the classification of proton conductors as a function of the water vapor partial pressure proposed by Colomban and Novak [35], the behavior of the membranes is somewhere between an intrinsic conductor (bulk conductor) and a surface conductor. The data show that the conductivity increases with RH, with the greatest increase observed between 58 and 81% RH. In both cases, the conductivity improves almost three orders of magnitude from 33 to 81%. The change in conductivity is from 1.38×10^{-6} S cm^{-1} at 33% RH ($\log_{10}\sigma = -5.86$) to 5.48×10^{-6} S cm^{-1} at 58% RH ($\log_{10}\sigma = -5.26$) and exhibits a sharp change (from 5.48×10^{-6} S cm^{-1} at 58% RH to 9.06×10^{-4} S cm^{-1} ($\log_{10}\sigma = -3.04$) at 81%, all data at 40 °C. Fig. 7 depicts the proton conductivity of the hematite xerogels at different relative humidities versus the reciprocal of temperature (from 25 to 90 °C). An Arrhenius-like dependence with temperature is observed in all cases. At 90 °C and 81% RH, the proton conductivity is 2.76×10^{-3} S cm^{-1}, the highest value observed. The values of the activation energy (E_a) were obtained by linear regression of the Arrhenius equation $\sigma = \sigma_0 \exp(-E_a/kT)$, where σ_0 is a pre-exponential parameter and k is the Boltzmann's constant. The activation energy values for each relative humidity are registered in Fig. 7. According to those values, proton migration can be dominated by the Grotthuss mechanism. In this mechanism, the proton forms a H_3O^+ ion and jumps to the neighboring lone pair of electrons of a water molecule. For such a mechanism, the activation energy for proton conduction should be about 0.14–0.40 eV [36]. The decrease in the activation energies when relative humidity increases (up to 75% RH) can be explained from the higher water content. The filling up of channels by water molecules leads to a higher conductivity, not only via the σ_0 factor, which is proportional to the number of mobile species, but also by increasing the dynamical disorder [36]. That is also confirmed by the water isothermal where it is observed that the number of water molecules is the same for both temperatures, 25 and 40 °C, as it is mentioned above.

Following Sumner et al. [37] and Zawodzisnki and Gottesfeld [38], the conductivity of Nafion does not depend as strongly on relative humidity as the α-Fe_2O_3 ceramic membranes. At room temperature, the values reported by Sumner et al. [37] range from 1.0×10^{-2} S cm^{-1} at 45% RH to 4.0×10^{-2} S cm^{-1} at 70% RH. At higher temperatures, the conductivity of Nafion® 117 does not increase at the same rate as it does with RH, and the value reported for Nafion® at 79 °C and 42% RH is 1.3×10^{-2} S cm^{-1}. Furthermore, Zawodzisnki and Gottesfeld [38] reported that the water content in Nafion® 117, in terms of water molecules per sulfonate group, does not change significantly when the temperature is raised from 30 to 80 °C in samples equilibrated with water vapor, and that the membranes takes up less water as the temperature is raised. We therefore assume that the same behavior can be expected under higher temperature and RH conditions. If we extrapolate Sumner's data to the same conditions used in our study, we find that the conductivity of Nafion® 117 is about 3.7×10^{-2} S cm^{-1}. Although the proton conductivity values of the hematite membranes are lower than that of Nafion® the ceramic membranes can be easily obtained as thinnest as it is needed [18], whereas Nafion® 111, the thinnest polymeric membranes are about 25 μm thick [39]. Therefore, the actual ohmic resistance of such ceramic membranes would be lower in a given device. In addition, the hematite ceramic membranes are not susceptible to deformation under sorption, desorption and, permeation of water unlike organic membranes.

Fig. 8 presents the hydrogen permeability values as a function of the reciprocal temperature for the hematite membrane. As the temperature increased from 25 to 100 °C the permeability values decreased from 5.21×10^{-9} to 9.24×10^{-10} mol (cm s Pa)$^{-1}$. These values are lower than that of Nafion® membrane 117 which is 3.01×10^{-13} mol (cm s Pa)$^{-1}$ at 30 °C [40]. Then, in order to fabricate oxide-based PEMs that are capable of keeping streams of H_2 and O_2 from mixing, a separation layer with pore sizes <2 nm whose pores are filled with water will be needed. If the mesoporous membrane is placed between two hematite microporous films in a sandwich configuration fuel cell, those thin films will serve as gas barriers to prevent the combination of fuel gas and oxidant gas. The proposed configuration is shown in Fig. 9.

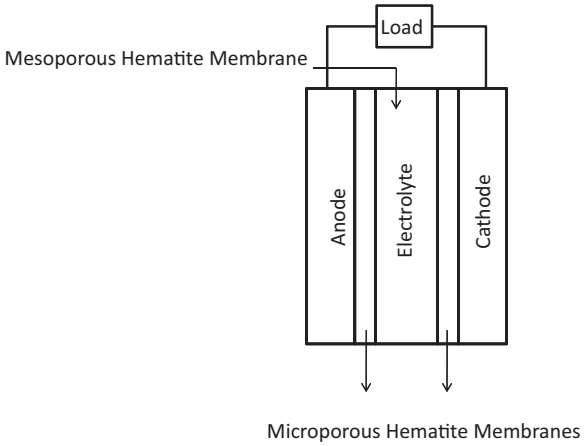

Fig. 9. Proposed configuration of an oxide-based PEM fuel cell.

4. Concluding remarks

In summary, the mesoporous acid-free hematite ceramic membranes synthesized have proton conductivity and water uptake behaviors with a sigmoidal dependence on RH, with the greatest increase observed between 58 and 81%. The proton conductivity shows an Arrhenius-like dependence on temperature for all RH studied. The highest value of proton conductivity was found to be 2.76×10^{-3} S cm^{-1} at 90 °C and 81% RH. According to the activation energy values (0.20–0.39 eV), proton migration can be dominated by the Grotthuss mechanism in the whole range of RH.

Conclusively, the proton conductivity values, environmental friendly behavior, lower cost and higher hydrophilicity of mesoporous hematite membranes make them potential substitutes for Nafion membranes in proton exchange membranes fuel cells (PEMFCs).

Although the proton conductivity values of the hematite membranes are lower than that of Nafion the ceramic membranes can be easily obtained thinner that the thinnest Nafion membranes (about 50–70 μm or even higher thick). Therefore, the actual ohmic resistance of such ceramic membranes would be lower in a given device.

Acknowledgements

The author wishes to acknowledge Miss K. Zenzinger for her help during the preparation of the samples. Part of this work was performed at the Environmental Chemistry and Technology Department (University of Wisconsin-Madison) in the frame of the contract DE-FC02-99EE50583 (US Department of Energy).

References

[1] R.M. Cornell, U. Schwertmann, The Iron Oxides, VCH Verlagsgesellschaft, Weinheim, Germany, 1996, p. 463.
[2] T. Hashimoto, T. Yoko, S. Saka, J. Ceram. Soc. Jpn. 101 (1993) 64.
[3] X.Q. Liu, S.W. Tao, Y.S. Shen, Sens. Actuators B 40 (1997) 161.
[4] L.A. Pérez-Maqueda, J.M. Criado, J. Subrt, C. Real, Cat. Lett. 60 (1999) 151.
[5] J.Y. Zhong, C.B. Cao, Sens. Actuators B: Chem. 145 (2010) 651.
[6] K. Hagedorn, C. Forgacs, S. Collins, S. Maldonado, J. Phys. Chem. C 114 (2010) 12010.
[7] K.D. Kreuer, Solid State Ionics 97 (1997) 1.
[8] A. Gruger, A. Régis, T. Schmatko, Ph. Colomban, Vib. Spectrosc. 26 (2001) 215.
[9] M. Nogami, R. Nagao, C. Wong, J. Phys. Chem. B 102 (1998) 5772.
[10] M. Nogami, Y. Goto, Y. Tsurita, T. Kasuga, J. Am. Ceram. Soc. 84 (2001) 2553.
[11] T. Ioroi, K. Kuraoka, K. Yasuda, T. Yazawa, Y. Miyazaki, Electrochem. Solid State Lett. 7 (2004) A394.
[12] F.M. Vichi, M.T. Colomer, M.A. Anderson, Electrochem. Solid State Lett. 2 (1999) 313.
[13] U.B. Mioc, S.K. Milonjic, V. Stamenkovic, M. Radojevic, Ph. Colomban, M.M. Mitrovic, R. Dimitrijevic, Solid State Ionics 125 (1999) 417.
[14] M.T. Colomer, M.A. Anderson, J. Non-Cryst. Solids 290 (2001) 93.
[15] A. Matsuda, T. Kanzaki, K. Tadanaga, M. Tatsumisago, T. Minami, Electrochim. Acta 47 (2001) 939.
[16] A.A. Anappara, S. Rajeshkumar, P. Mukundan, P.R.S. Warrier, S. Ghosh, K.G.K. Warrier, Acta Mater. 52 (2004) 369.
[17] M.T. Colomer, J. Eur. Ceram. Soc. 26 (2006) 1231.
[18] M.T. Colomer, Adv. Mater. 18 (2006) 371.
[19] M.T. Colomer, F. Rubio, J.R. Jurado, J. Power Sources 167 (2007) 53.
[20] S.M. Haile, D.A. Boysen, C.R.I. Chisholm, R.B. Merle, Nature 410 (2001) 910.
[21] R.B. Merle, C.R.I. Chisholm, D.A. Boysen, S.M. Haile, Energy Fuels 17 (2003) 210.
[22] S. Lu, D. Wang, S.P. Jing, Y. Xiang, J. Lu, J. Zeng, Adv. Mater. 22 (2010) 971.
[23] K.S.W. Sing, D.H. Everett, R.A.W. Haul, L. Moscou, R.A. Pierotti, J. Rouquerol, T. Siemieniewska, Pure Appl. Chem. 57 (1985) 603.
[24] E.P. Barret, L.G. Joyney, P.P. Halenda, J. Am. Chem. Soc. 73 (1951) 373.
[25] N.A. Seaton, Chem. Eng. Sci. 46 (1991) 1895.
[26] David R. Lide (Editor-in-Chief), Handbook of Chemistry and Physics, 84th ed., CRC Press, 2003–2004.
[27] B. Boukamp, Equivalent Circuit (EQUIVCRT.PAS), University of Twente, Twente, The Netherlands, 1988–1989.
[28] J.L. Rendon, J. Cornejo, P. de Arambarri, C.J. Serna, J. Colloid Interface Sci. 92 (1983) 508.
[29] J.H. de Boer, in: D.H. Everett, F.S. Stone (Eds.), The Structure and Properties of Porous Materials, Butterworths, London, 1958, p. 195.
[30] S.J. Gregg, K.S.W. Sing, Adsorption, Surface Area Porosity, Academic Press, London, 1982.
[31] I.I. Salame, T.J. Bandosz, Langmuir 15 (1999) 587.
[32] C.-L. McCallum, T.J. Bandosz, S.C. McGrother, E.A. Müller, K.E. Gubbins, Langmuir 12 (1996) 533.
[33] M.M. Dubinin, W. Serpinsky, J. Colloid Interface Sci. 21 (1966) 378.
[34] M. Nogami, H. Matsushita, T. Kasuga, T. Hayakawa, Electrochem. Solid State Lett. 2 (1999) 415.
[35] P. Colomban, A. Novak, in: P. Colomban (Ed.), Proton Conductors, Cambridge University, Cambridge, 1992, pp. 38–55.
[36] K.D. Kreuer, I. Stoll, A. Rabenau, Solid State Ionics 9–10 (1983) 1061.
[37] J.J. Sumner, S.E. Creager, J.J. Ma, D.D. DesMarteau, J. Electrochem. Soc. 145 (1998) 107.
[38] T.A. Zawodzisnki Jr., S. Gottesfeld, Abstract 94, The Electrochemical Society Extended Abstracts, Toronto, Ontario, Canada, 1992, pp. 11–16.
[39] L. Wu, C. Huang, J.-J. Woo, D. Wu, S.-H. Yun, S.-J. Seo, T. Xu, S.-H. Moon, J. Phys. Chem. B 113 (2009) 12265.
[40] G. Lakshminarayana, M. Nogami, I.V. Kityk, Energy 35 (2010) 5260.